Classification of stable Dirac and Weyl semimetals with reflection and rotational symmetry

Zihao Gao,[1] Meng Hua,[1] Haijun Zhang,[2] and Xiao Zhang[1,*]

[1]*Department of Physics, Sun-Yat-Sen University, Guangzhou, China*

[2]*National Laboratory of Solid State Microstructures, School of Physics, Collaborative Innovation Center of Advanced Microstructures, Nanjing University, Nanjing 210093, China*

(Received 17 November 2015; revised manuscript received 28 March 2016; published 9 May 2016)

Three-dimensional (3D) Dirac and Weyl semimetals are novel states of quantum matter. We classify stable 3D Dirac and Weyl semimetals with reflection and rotational symmetry in the presence of time reversal symmetry and spin-orbit coupling, which belong to seventeen different point groups. They have two classes of reflection symmetry, with the mirror plane parallel and perpendicular to rotation axis. In both cases two types of Dirac points, existing through accidental band crossing (ABC) or at a time reversal invariant momentum (TBC), are determined by four different reflection symmetries. We classify those two types of Dirac points with a combination of different reflection and rotational symmetries. We further classify Dirac and Weyl line nodes to show in which types of mirror plane they can exist. Finally we discuss that Weyl line nodes and Dirac points can exist at the same time taking C_{4v} symmetry as an example.

DOI: 10.1103/PhysRevB.93.205109

I. INTRODUCTION

Dirac semimetals are new states of quantum matter. They have gap closing (points or line nodes) of conduction and valence band which show pseudorelativistic physics of 3D Dirac fermions near the Fermi energy. Before the discovery of Dirac semimetals, the topological quantum states, such as 3D topological insulator [1,2], have two-dimensional (2D) Dirac fermions on the surface. Different from topological insulators and superconductors, Dirac semimetals hold nontrivial features in the bulk states [3–22].

Stable 3D Dirac semimetals have been theoretically predicted [5,17] and observed experimentally in Cd_3As_2 and Na_3Bi [18–22] by angle-resolved photoemission spectroscopy (ARPES). In these materials there are two stable Dirac points (DPs) in the k_z axis stabilized by rotational symmetry. While in β-cristobalite structure such like BiO_2 [3], the DPs exist at a time reversal invariant momentum (TRIM). Recently, a new type of Dirac semimetal, Dirac line nodes (DLNs), has been proposed in $AIrO_3$, 3D graphene networks, LaN, and Cu_3NPd [6–13]. DLNs can exist in the system with or without spin-orbit coupling (SOC) [23]. Meanwhile, theoretical prediction shows that time reversal symmetry (TRS) breaking systems including $HgCr_2Se_4$ [24] has Weyl nodes and a Weyl line node (WLN) in its mirror plane. Also systems with TRS breaking such as pyrochlore iridates [25] and $(CdO)_2(EuO)_2$ [26] or with TRS such as TaAs, NbAs, NbP, TaP and WTe_2 [27–39] have Weyl nodes.

Inspired by these works, we ask which point group can protect Dirac and Weyl semimetals. Only ten out of thirty-two point groups have both inversion and rotational symmetry which have been classified [40]. Here we classify 3D stable DPs and newly predicted DLN [23] and WLN [24] in the systems preserving TRS, reflection symmetry, and uniaxial rotational symmetry, which include seventeen point groups both with and w/o inversion symmetry. Known that the reflection symmetry plays an important role in classification of topological phases [41–43], we first study the classification of reflection symmetries in seventeen different point groups, covering all point groups with inversion symmetry apart from C_{3i}. There are two classes of reflection symmetry, with the mirror plane parallel and perpendicular to rotation axis. In both cases two types of DPs, created by ABC or by TBC, are determined by four different reflection symmetries. Then we show that in both mirror parallel and perpendicular cases, $C_{2,3}$ symmetry can only protect stable DPs via TBC, while $C_{4,6}$ symmetry can have stable DPs as ABC or TBC. We further classify DLNs and WLNs to show in which types of mirror plane they can exist. Finally we discuss the coexistence of DPs and WLNs.

II. HAMILTONIAN

A 4×4 Hamiltonian describing the four energy bands of a system preserving TRS and uniaxis rotational symmetry in a general form,

$$H=\begin{pmatrix} h_{\uparrow\uparrow}(\vec{k}) & h_{\uparrow\downarrow}(\vec{k})\\ h_{\downarrow\uparrow}(\vec{k}) & h_{\downarrow\downarrow}(\vec{k})\end{pmatrix}=\sum_{i,j=0}^{3} a_{ij}(\vec{k})\tau_i\sigma_j,$$

where σ_i represents the spin space and τ_i represents orbital space. $h_{\sigma\sigma'}(\sigma=\uparrow,\downarrow)$ is a 2×2 matrix and $\uparrow\downarrow$ represent opposite spin in k_z direction. All the $a_{ij}(\vec{k})$ are real functions and we can determine the parity of each coefficient $a_{ij}(\vec{k})$ through TRS $H(-\vec{k})=TH(\vec{k})T^{-1}$, where $T=i\sigma_y K$. The system is invariant under C_n rotational symmetry which gives $C_nH(\vec{k})C_n^{-1}=H(R_n\vec{k})$, where R_n is the rotation operator for 3D n-fold rotation in k space and the basis vectors are chosen to be eigenstates of C_n. We choose the rotation axis as the k_z axis, therefore $R_nk_z=k_z$. Rotational symmetry suggests commutation relation $C_nH(k_z)C_n^{-1}=H(k_z)$ on the k_z axis between the Hamiltonian $H(k_z)$ and C_n operators. Therefore we choose a basis to make C_n a diagonal form $C_n=\mathrm{diag}(\alpha_p,\alpha_q,\alpha_r,\alpha_s)$, where $\alpha_p=\exp[i\frac{2\pi}{n}(p+\frac{1}{2})]$, p is the effective orbital angular momentum for rotational symmetry. Here each basis vector is a C_n rotation eigenstate and has a definite rotation eigenvalue $p+\frac{1}{2}$.

*zhangxiao@mail.sysu.edu.cn

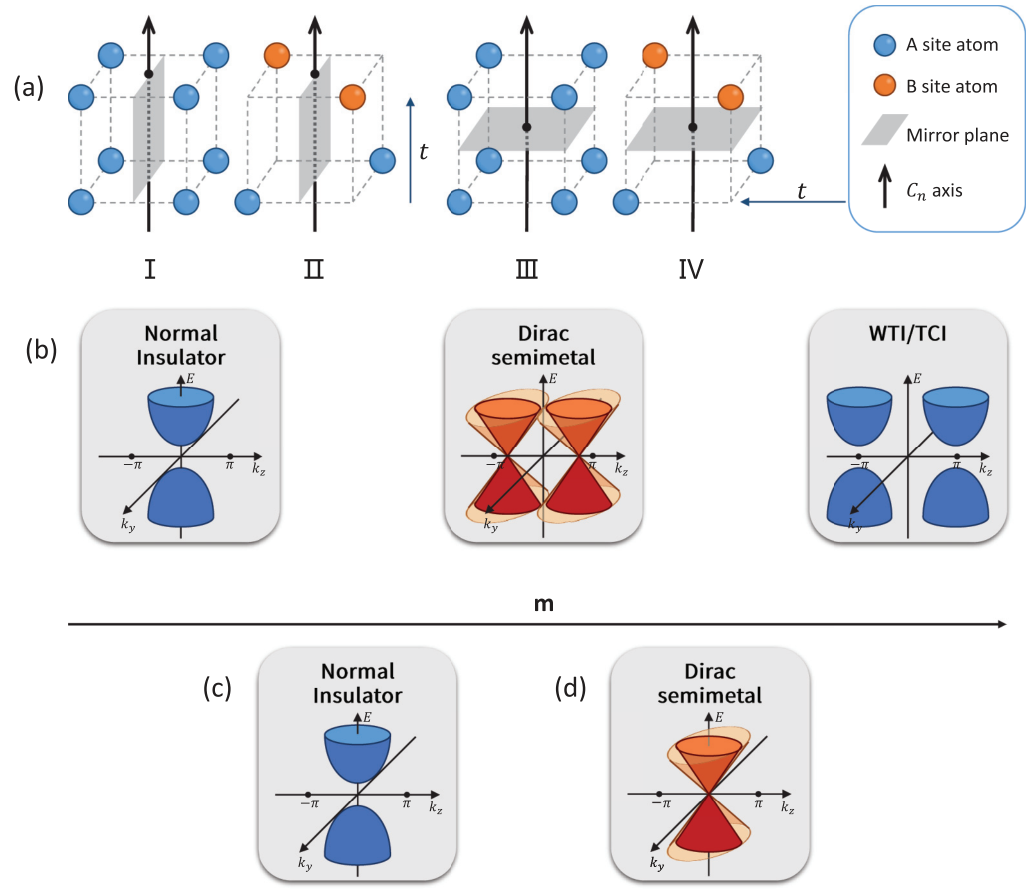

FIG. 1. (a) Schematic diagrams of reflection symmetries in space groups: the mirror plane parallel to rotation axis as shown in a_I and a_{II} and the mirror plane perpendicular to rotation axis as shown in a_{III} and a_{IV}. The reflection operators are not the same as the intuitive ones because of the phase factor stemming from spin. In both cases, for normal mirror plane a_I and a_{III}, there is only one equivalent site. As for glide mirror plane a_{II} and a_{IV}, which are reflection symmetries with t translation, there are two inequivalent sites in the lattice. (b) The phase transition determined by a control parameter m and Dirac semimetal created by accidental band crossing (ABC). When m is in a proper range, two Dirac points show up on the k_z axis. This phase lays between two gapped phase such as normal insulator and weak topological insulator (WTI)/topological crystalline insulator (TCI). (c) For ABC, when the conduction band and valence band have the same rotation eigenvalue, i.e., $p = q$, they will never cross each other because of strong level repulsion. (d) The Dirac semimetal phase is protected by crystalline symmetry (TBC).

III. CLASSIFICATION OF REFLECTION SYMMETRY

Point groups with reflection symmetries can be distinguished in two classes by the relative positions between the mirror plane and rotation axis k_z: In the first class, k_z axis parallels the mirror plane, and the system doesn't preserve inversion symmetry which correspond to point groups $C_{2v}, C_{3v}, C_{4v}, C_{6v}$, D_{2d}, and T_d. In these systems, reflection symmetry can be a point group symmetry as shown in Fig. 1.(a_{I}) or a nonsymmorphic glide plane symmetry which is the combination of a reflection operation and a translation t as shown in Fig. 1.(a_{II}). Neupane *et al.* [18] realized Dirac semimetal Cd_3As_2 which belongs to nonsymmorphic space group $I4_1cd$ (C_{4v}). Whereas in the second class, when the k_z axis is perpendicular to the mirror plane, inversion symmetry will emerge through the combination of reflection symmetry and C_2 rotational symmetry [40,44]. Here the point group reflection symmetry is shown in Fig. 1. (a_{III}) and the glide plane symmetry in nonsymmorphic space group is shown in Fig. 1.(a_{IV}).

Mirror operator is an inversion operation followed by a C_2 rotation whose rotation axis is perpendicular to the mirror plane. It should satisfy the following constraints: (1) $[M,T] = 0$, (2) $M^{+}M = 1$, (3) $MM = e^{i\phi}$. If we set the mirror plane as the yz plane or xy plane, the reflection operators will have the form: (A) $M_k = \pm\tau_0 \otimes i\sigma_k$, (B) $M_k = \pm\tau_z \otimes i\sigma_k$, (C) $M_k = \pm\tau_x \otimes i\sigma_k$, and (D) $M_k = \pm i\tau_y \otimes i\sigma_k$ $(k = x,z)$. They are not the same as the intuitive mirror operators because of the phase generated by spin. It is also worth mentioning that the subtle reflection operator $M_k = \pm i\tau_y \otimes i\sigma_k$ can be constructed through glide mirror operation with a translation. Glide plane operator will produce a phase factor after being applied twice. (See Appendix B for detailed examples.) Note that the basis in our framework is after considering spin-orbit coupling (SOC).

IV. CLASSIFICATION TABLE OF STABLE DIRAC POINTS

After applying TRS and rotational symmetry, the Hamiltonian in k_z axis becomes a diagonal form with the above

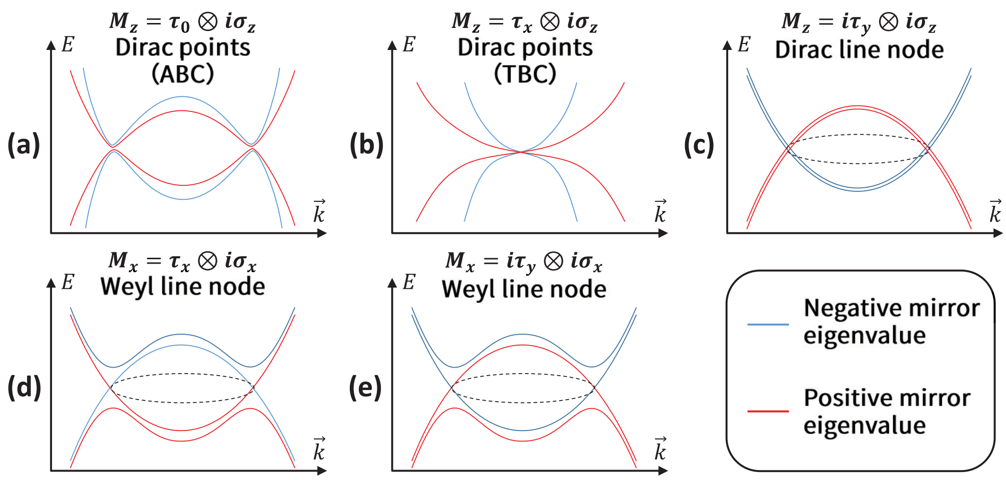

FIG. 2. Dirac or Weyl semimetals protected by reflection symmetry. (**a**),(**b**) Examples of Dirac points as ABC (**a**) and TBC (**b**). (**c**) For mirror $M_z = i\tau_y \otimes i\sigma_z$, conduction (valence) band consists of two bands with the same mirror eigenvalues. There isn't level repulsion between conduction and valence bands and the crossing of two bands generates a DLN. (**d**),(**e**) For various kinds of mirrors (e.g., $i\tau_y \otimes i\sigma_x$ and $\tau_x \otimes i\sigma_x$), WLNs can be protected as long as the crossing bands have different mirror eigenvalues and so level repulsion doesn't happen (Table IV).

basis

$$H(k_z) = a_{00} + a_{03}\sigma_3 + a_{33}\tau_3\sigma_3 + a_{30}\tau_3. \qquad (1)$$

The DPs are created only when $a_{03,33,30}(k_z,m) = 0$, where m is a control parameter. There are three equations and two variables, so we need additional symmetry constraints to guarantee these equations having at least one solution that can generate stable DPs. After we impose reflection symmetry, $H(k_z)$ can be further constrained and will reveal the Dirac semimetal phase. As shown in the Appendix, different reflection operators will hold different types of DPs. When the reflection operator is $M_k = \tau_0/\tau_z \otimes i\sigma_k (k = x,z)$, only $a_{30}(k_z,m)$ survives. $a_{30}(k_z)$ is an even function with respect to k_z, so $a_{30}(k_z,m) \approx M_0 - M_1 k_z^2$ for the leading order. Two DPs will emerge in the k_z axis at $k_z = \pm\sqrt{M_0/M_1}$. This kind of Dirac semimetal is created through the two bands accidentally crossing each other (ABC) when the conduction band and valence band have different rotation eigenvalues ($p \neq q$).

TABLE I. Classification table of Dirac points when k_z is parallel to mirror plane. Here we choose k_z as the rotation axis and assume that the yz plane is a mirror plane. (p,q,r,s) can be regarded as a set of orbital angular momentum in z direction and j is the total angular momentum. For compact presentation, we assume $n/2 \leqslant q \leqslant p < n$ and consider the equivalence between $\{p,r\}$ and $\{q,s\}$. The 2×2 Hamiltonian $h_{\uparrow\uparrow}(\vec{k}) = f_0(\vec{k}) + f_+(\vec{k})\tau_+ + f_-(\vec{k})\tau_- + f_z(\vec{k})\tau_z$, and $h_{\uparrow\downarrow}(\vec{k}) = g_0(\vec{k}) + g_+(\vec{k})\tau_+ + g_-(\vec{k})\tau_- + g_z(\vec{k})\tau_z$. The leading order of $f_\pm, g_\pm, g_0+g_z, g_0-g_z$ are shown in the table. Each term should be multiplied by an coefficient function of k_z respecting to the parity of $a_{ij}(k)$ when constructing the elements of the Hamiltonian.

M_x	C_n	(p,q,r,s)	Total j	$f_\pm$	$g_\pm$	g_0+g_z	g_0-g_z	Dirac Type	Materials	Dispersion in k_y
$\pm\tau_0/\tau_z$	C_2/C_3									
	C_4	(3,2,0,1)	$(\pm\frac{1}{2},\pm\frac{3}{2})$	k_+	$k_\pm^2$	k_-	k_+	ABC	$Cd_3As_2(I4_1cd)$	Linear Dirac
	C_6	(5,4,0,1)	$(\pm\frac{1}{2},\pm\frac{3}{2})$	k_+	k_-^2	k_-	$k_\pm^3$	ABC		Linear Dirac
	C_6	(5,3,0,2)	$(\pm\frac{1}{2},\pm\frac{5}{2})$	k_+^2	$k_\pm^3$	k_-	k_+	ABC		Linear Dirac
	C_6	(4,3,1,2)	$(\pm\frac{3}{2},\pm\frac{5}{2})$	k_+	k_+^2	$k_\pm^3$	k_+	ABC		Linear Dirac
$\pm\tau_x$	C_2									
$\pm\tau_x/i\tau_y$	C_3	(2,1,0,1)	$(\pm\frac{1}{2},\pm\frac{3}{2})$	k_+	k_+	k_-	k_+k_-	TBC		Linear Dirac
	C_4	(3,2,0,1)	$(\pm\frac{1}{2},\pm\frac{3}{2})$	k_+	$k_\pm^2$	k_-	k_+	TBC		Linear Dirac
	C_6	(5,4,0,1)	$(\pm\frac{1}{2},\pm\frac{3}{2})$	k_+	k_-^2	k_-	$k_\pm^3$	TBC		Linear Dirac
	C_6	(5,3,0,2)	$(\pm\frac{1}{2},\pm\frac{5}{2})$	k_+^2	$k_\pm^3$	k_-	k_+	TBC		Linear Dirac
	C_6	(4,3,1,2)	$(\pm\frac{3}{2},\pm\frac{5}{2})$	k_+	k_+^2	$k_\pm^3$	k_+	TBC		Linear Dirac
$\pm i\tau_y$	C_2	(1,1,0,0)	$(\pm\frac{1}{2},\pm\frac{1}{2})$	k_+k_-	k_+	$k_\pm$	$k_\pm$	TBC		Linear Dirac
	C_3	(2,2,0,0)	$(\pm\frac{1}{2},\pm\frac{1}{2})$	k_+k_-	k_-	k_-	k_-	TBC		Linear Dirac
	C_4	(3,3,0,0)	$(\pm\frac{1}{2},\pm\frac{1}{2})$	k_+k_-	k_-	k_-	k_-	TBC		Linear Dirac
	C_4	(2,2,1,1)	$(\pm\frac{3}{2},\pm\frac{3}{2})$	k_+k_-	k_+	k_+	k_+	TBC		Linear Dirac
	C_6	(5,5,0,0)	$(\pm\frac{1}{2},\pm\frac{1}{2})$	k_+k_-	k_-	k_-	k_-	TBC		Linear Dirac
	C_6	(4,4,1,1)	$(\pm\frac{3}{2},\pm\frac{3}{2})$	k_+k_-	$k_\pm^3$	$k_\pm^3$	$k_\pm^3$	TBC		Quadratic Dirac
	C_6	(3,3,2,2)	$(\pm\frac{5}{2},\pm\frac{5}{2})$	k_+k_-	k_+	k_+	k_+	TBC		Linear Dirac

TABLE II. Classification table of Dirac points when k_z is perpendicular to the mirror plane. Here we choose k_z as the rotation axis and assume that the xy plane is a mirror plane. We use the same notation as in Table I. For compact presentation, we assume $q \leqslant p < n$ and consider the equivalence between $\{p,r\}$ and $\{q,s\}$.

M_z	C_2	P	C_n	(p,q,r,s)	Total j	$f_\pm$	$g_\pm$	$g_0 \pm g_z$	Dirac Type	Materials	Dispersion in k_y
τ_0/τ_z	τ_0	τ_0/τ_z	C_2								
			C_4	(2,0,1,3)	$(\pm\frac{3}{2},\pm\frac{1}{2})$	$k_\pm^2$	k_+	0	ABC	$Cd_3As_2(I4_1acd)$	Linear
			C_6	(2,0,3,5)	$(\pm\frac{5}{2},\pm\frac{1}{2})$	k_+^2	$k_\pm^3$	0	ABC		Quadratic
			C_6	(3,1,2,4)	$(\pm\frac{5}{2},\pm\frac{3}{2})$	k_+^2	k_-	0	ABC		Linear
			C_6	(4,0,1,5)	$(\pm\frac{3}{2},\pm\frac{1}{2})$	k_-^2	k_-	0	ABC		Linear
	τ_z	τ_z/τ_0	C_2								
			C_4	(1,0,2,3)	$(\pm\frac{3}{2},\pm\frac{1}{2})$	k_+	$k_\pm^2$	0	ABC		Linear
			C_6	(1,0,4,5)	$(\pm\frac{3}{2},\pm\frac{1}{2})$	k_+	k_+^2	0	ABC		Linear
			C_6	(2,1,3,4)	$(\pm\frac{5}{2},\pm\frac{3}{2})$	k_+	k_-^2	0	ABC		Linear
			C_6	(3,0,2,5)	$(\pm\frac{5}{2},\pm\frac{1}{2})$	$k_\pm^3$	k_-^2	0	ABC		Quadratic
$i\tau_y$	τ_0	$i\tau_y$	C_2/C_6								
			C_4	(2,0,1,3)	$(\pm\frac{3}{2},\pm\frac{1}{2})$	$k_\pm^2$	k_-	k_+	TBC		Linear
	τ_z	τ_x	C_2	(1,0,0,1)	$(\pm\frac{1}{2},\pm\frac{1}{2})$	$k_\pm$	0	$k_\pm$	TBC	Distorted spinels [45]	Linear
			C_4								
			C_6	(3,0,2,5)	$(\pm\frac{5}{2},\pm\frac{1}{2})$	$k_\pm^3$	0	k_+	TBC		Linear
			C_6	(4,1,1,4)	$(\pm\frac{3}{2},\pm\frac{3}{2})$	$k_\pm^3$	0	$k_\pm^3$	TBC		Cubic
τ_x	τ_0	τ_x	C_2/C_6								
			C_4	(2,0,1,3)	$(\pm\frac{3}{2},\pm\frac{1}{2})$	$k_\pm^2$	0	k_+	TBC	BiO_2	Linear
	τ_z	$i\tau_y$	C_2/C_4								
			C_6	(3,0,2,5)	$(\pm\frac{5}{2},\pm\frac{1}{2})$	$k_\pm^3$	k_-^2	k_+	TBC		Linear

It can be understood as a phase between normal insulator and weak topological insulator (WTI) [46–48]/topological crystalline insulator (TCI) [49,50] [Fig. 2(a)]. When reflection operator is $M_k = i\tau_y/\tau_x \otimes i\sigma_k$, only $a_{33}(k_z,m)$ survives which is an odd function with respect to k_z. The leading order is $a_{33} = M_2 k_z$. There is one Dirac point at TRIM (TBC) generated by band crossing. Under this scenario, the DPs are created and stabilized by the crystalline symmetry [Fig. 2(b)]. We will use the tables below to show the physical properties of all kinds of DPs.

The classification of DPs when the mirror plane is parallel to the k_z axis is shown in Table I. C_2 and C_3 rotational systems can only generate DPs via TBC. C_4 and C_6 symmetries can protect DPs as ABC or TBC in the presence of all those four reflection symmetries. Table II demonstrate the classification of 3D DPs when the mirror plane is perpendicular to the k_z axis. Inversion symmetry can emerge through $P = C_2 m_z$, where C_2 is a twofold rotation along the k_z axis in systems preserving C_2, C_4, C_6 symmetry. Yang and Nagaosa [40] have already considered unitary inversion operator $P = \tau_0, \tau_x, \tau_z$. We show that in Table II the same results hold when inversion operators are unitary. However, the mirror operators can also generate the antiunitary inversion operator $P = i\tau_y$. $P = i\tau_y$ is an inversion operator with a translation in nonsymmorphic space groups. Similar to Table I, C_2 rotational systems can only generate DPs via TBC, and C_4 and C_6 symmetries can protect DPs as ABC or TBC in the presence of all those four reflection symmetries in combination with certain rotational eigenvalues. One special case is the D_{3h} group, which does not involve inversion symmetry. As shown in Table III, only $M_z = i\tau_y \otimes i\sigma_z$ can protect a Dirac point at TRIM.

V. DIRAC AND WEYL LINE NODES IN MIRROR PLANE

DLNs [23] in the mirror plane emerge in systems with inversion, TRS, and reflection symmetry. Due to the combination of inversion symmetry and TRS, two bands related by TRS actually stick together and make up a twofold degenerate band. When we study the Hamiltonian in the mirror plane, if the conduction (valence) band consists of two bands with different mirror eigenvalues, the bands with the same (positive or negative) mirror eigenvalue from the conduction and valence bands will have strong level repulsion and open up a gap [Figs. 2(a) and 2(b)]. Otherwise when the sub-bands have

TABLE III. Classification table of topological phase for D_{3h}. Here we choose k_z as the rotation axis and assume that the xy plane is a mirror plane. For compact presentation, we assume $q \leqslant p < n$ and consider the equivalence between $\{p,r\}$ and $\{q,s\}$.

M_z	C_n	(p,q,r,s)	Total j	$f_\pm$	$g_\pm$	$g_0 + g_z$	$g_0 - g_z$	Dirac Type	Dispersion in k_y direction
$i\tau_y$	C_3	(2,0,0,2)	$(\pm\frac{1}{2},\pm\frac{1}{2})$	k_-	0	k_-	k_+	TBC	Linear Dirac
	C_3	(2,1,0,1)	$(\pm\frac{1}{2},\pm\frac{3}{2})$	k_+	0	k_-	k_+k_-	TBC	Linear Dirac

TABLE IV. The possible protected semimetal phases by reflection symmetry. The reflection operators with σ_x stands for mirror parallel to rotation axis z and σ_z for mirror perpendicular to rotation axis z. ($k = x,z$.)

Mirror operator	ABC	TBC	WLN	DLN
$\tau_0 \otimes i\sigma_k$	√		√	
$\tau_x \otimes i\sigma_k$		√	√	
$i\tau_y \otimes i\sigma_k$		√	√	√
$\tau_z \otimes i\sigma_k$	√		√	

the same mirror eigenvalues, the conduction band will have a different mirror eigenvalue from the valence band, and the level repulsion will be relaxed [Fig. 2(c)]. The band crossing will create DLNs in the mirror plane which can only be protected by the nonsymmorphic reflection operators $M_{x,z} = \pm i\tau_y \otimes i\sigma_{x,z}$ (Table IV). For $SrIrO_3$ with SOC of space group #62, DLN is located around point $U(0,\pi,\pi)$ of the mirror plane $k_y = \pi$ in the Brillouin zone [6,23], which belongs to this type of reflection.

Either breaking inversion symmetry or TRS can produce Weyl semimetals. Different from WLNs in $HgCr_2Se_4$ [24] and $(CdO)_2(EuO)_2$ [26], which breaks TRS, we construct WLNs in the presence of TRS. WLNs are protected when the crossing bands have different mirror eigenvalues. As is shown in [Figs. 2(d) and 2(e)] and Table IV, WLNs may emerge on various kinds of mirror plane because of its twofold degeneracy nature. Note that DLNs and WLNs protected by mirror symmetry also apply to two-dimensional systems, because in 3D systems we just take a plane in the Brillouin zone into consideration.

VI. THE COEXISTENCE OF DIRAC POINTS AND WEYL LINE NODES

For now we can construct DPs in the systems preserving reflection symmetry but without inversion symmetry. We expect in some cases DPs and WLNs can exist simultaneously with SOC. We illustrate this distinctive properties in materials with C_{4v} point group like Cd_3As_2 with angular momentum $(\pm\frac{1}{2},\pm\frac{3}{2})$ through $k \cdot p$ perturbation method. The detailed calculations are shown in the Appendix. By choosing some proper parameters, the band structure shown in Figs. 3(a) and 3(b) exhibits two DPs along the Γ-Z direction and two WLNs in the yz plane and xz plane. Figure 3(c) shows the phase transition between different topological phases. Obviously the phase transition of WLNs is independent of the emergence of DPs in k_z direction. The simultaneous appearance of DPs and WLNs indicates a new class of topological phase with TRS and SOC.

This $k \cdot p$ Hamiltonian can have different topological phases depending on the SOC term D_0 and inversion breaking term B_0. In the gray area, the system breaks inversion symmetry but cannot protect Weyl semimetal. In the blue areas depending on the value of A_0, the conduction band and valence band will cross to form a WLN. When the inversion breaking term B_0 is small, the system will not have WLNs phase, but it can protect Dirac semimetal phase just like in $Cd_3As_2(I4_1acd)$. This phase diagram is independent of the creation of the Dirac semimetal phase in bulk band structure. Numerical calculation shows that the two crossing bands of WLNs in blue areas have different mirror eigenvalues, which protects the gap closing on the WLNs.

VII. CONCLUSION

We show that reflection symmetry can protect Dirac and Weyl semimetal phases with or without inversion symmetry. We have classified these phases in systems preserving reflection, rotational symmetry, and TRS. Table IV can be referred to for an overall possible protection of semimetal phases by reflection symmetry. There are two kinds of DPs created via ABC and TBC. In C_2 and C_3 rotation invariant systems, DPs can be created only via TBC. Whereas in C_4 and C_6 systems, DPs can be created via not only ABC but also TBC. We also show that DLNs in mirror plane can be protected only by $M_z = i\tau_y \otimes i\sigma_{x,z}$ and WLNs can be protected by any reflection

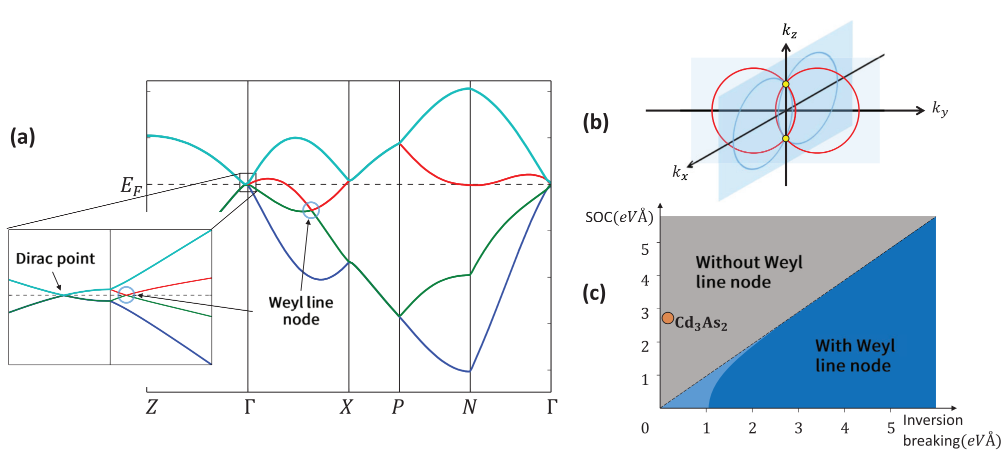

FIG. 3. (a) The electronic structure of C_{4v} system with SOC from $k \cdot p$ model shows the coexistence of Dirac points and WLNs. (b) Schematic diagram of the distribution of Dirac points (yellow points) and WLNs (red or blue circles) in the Brillouin zone. Dirac points locate on the interception of four WLNs. (c) Phase diagram with respect to B_0 (inversion breaking term), D_0 (SOC) and A_0 results from the $k \cdot p$ model. WLNs exist in the blue areas, among which the dark blue area represents the situation when the parameter $A_0 = -0.06$ eV (Cd_3As_2) [19] and the light blue area (partially covered by the dark one) for $A_0 = -0.00922$ eV (HgTe) [51].

operator. Finally, we find that in C_{4v} point group system, Dirac semimetal phase can coexist with WLNs. These new classes of Dirac and Weyl semimetals in inversion breaking and preserving systems can guide the search for novel materials with exotic quantum properties [52–57] and applications [58].

ACKNOWLEDGMENTS

We thank Ching Hua Lee for helpful discussions. X.Z. is support by the National Natural Science Foundation of China (No. 11404413), the Natural Science Foundation of Guangdong Province (No. 2015A030313188) and the Special Program for Applied Research on Super Computation of the NSFC-Guangdong Joint Fund (the second phase). M.H. and Z.G. acknowledge financial support from Yat-sen school, Sun Yat-sen University.

Z.G. and M.H. are contributed equally to this work.

APPENDIX A: HAMILTONIAN CONSTRAINED BY TIME REVERSAL SYMMETRY AND ROTATIONAL SYMMETRY

In this section we first constrain the Hamiltonian with time reversal symmetry (TRS) and rotational symmetry. Then we impose rotational symmetry C_n to the whole system to determine the leading order of the elements in $h_{\uparrow\uparrow}(\vec{k})$ and $h_{\uparrow\downarrow}(\vec{k})$. The Hamiltonian and the basis we use here is the same as that in the main text. Time reversal symmetry will constrain the Hamiltonian $H(\vec{k})$: $H(-\vec{k}) = TH(\vec{k})T^{-1}$, where the time reversal operator $T = i\sigma_y K$. We will have [40]

$$H = \begin{pmatrix} h_{\uparrow\uparrow}(\vec{k}) & h_{\uparrow\downarrow}(\vec{k}) \\ -h^*_{\uparrow\downarrow}(-\vec{k}) & h^*_{\uparrow\uparrow}(-\vec{k}) \end{pmatrix}.$$

At the same time, we know the parity of each coefficient with respect to momentum $a_{01,02,03,11,12,13,20,31,32,33}(-\vec{k}) = -a_{01,02,03,11,12,13,20,31,32,33}(\vec{k})$ and $a_{00,10,21,22,23,30}(-\vec{k}) = a_{00,10,21,22,23,30}(\vec{k})$. We set the rotation axis as k_z and choose the eigenstates of the rotation operator C_n as the basis of matrices. Then the matrix representation of C_n is

$$\begin{aligned} C_n &= \mathrm{diag}[\alpha_p,\alpha_q,\alpha_r,\alpha_s] \\ &= \begin{pmatrix} e^{i\frac{2\pi}{n}(p+1/2)} & 0 & 0 & 0 \\ 0 & e^{i\frac{2\pi}{n}(q+1/2)} & 0 & 0 \\ 0 & 0 & e^{i\frac{2\pi}{n}(r+1/2)} & 0 \\ 0 & 0 & 0 & e^{i\frac{2\pi}{n}(s+1/2)} \end{pmatrix} \\ &= \begin{pmatrix} e^{i\pi(\frac{1+p+q}{n}+\frac{p-q}{n}\tau_z)} & 0 \\ 0 & e^{i\pi(\frac{1+r+s}{n}+\frac{r-s}{n}\tau_z)} \end{pmatrix} \end{aligned} \tag{A1}$$

where $p,q,r,s \in \{0,1,\ldots,n-1\}$ and can be regarded as effective orbital angular momentum of different states. In general, C_n commutes with TRS $[C_n,T]=0$, thus p and r, q and s are related by:

$$\begin{aligned} &\alpha_p = \bar{\alpha_r}, \quad \alpha_q = \bar{\alpha_s} \\ &\exp\left[i\frac{2\pi}{n}(p+r+1)\right] = 1, \quad \exp\left[i\frac{2\pi}{n}(q+s+1)\right] = 1. \end{aligned} \tag{A2}$$

Next we derive the constraint relations between rotational symmetry and elements of the Hamiltonian. The 2×2 block Hamiltonian $h_{\uparrow\uparrow}$,$h_{\uparrow\downarrow}$ can be expanded in the following way [59]:

$$\begin{aligned} h_{\uparrow\uparrow}(\vec{k}) &= f_0(\vec{k}) + f_+(\vec{k})\tau_+ + f_+^*(\vec{k})\tau_- + f_z(\vec{k})\tau_z \\ h_{\uparrow\downarrow}(\vec{k}) &= g_0(\vec{k}) + g_+(\vec{k})\tau_+ + g_-(\vec{k})\tau_- + g_z(\vec{k})\tau_z \end{aligned} \tag{A3}$$

where $\tau_\pm = \tau_x \pm i\tau_y$, $f_{0,z}$ are real functions and $f_+,g_0,g_z,g_\pm$ are complex functions. Then the rotational symmetry $C_nH(k_\pm,k_z)C_n^{-1} = H(k_\pm e^{\pm i2\pi/n},k_z)$ gives the constraints of elements of the Hamiltonian:

$$\begin{aligned} f_z(k_\pm,k_z) &= f_z(k_\pm e^{\pm i2\pi/n},k_z) \\ \exp\left[i\frac{2\pi}{n}(p-q)\right]f_+(k_\pm,k_z) &= f_+(k_\pm e^{\pm i2\pi/n},k_z) \\ \exp\left[i\frac{2\pi}{n}(p-r)\right]g_{0+z}(k_\pm,k_z) &= g_{0+z}(k_\pm e^{\pm i2\pi/n},k_z) \\ \exp\left[i\frac{2\pi}{n}(q-s)\right]g_{0-z}(k_\pm,k_z) &= g_{0-z}(k_\pm e^{\pm i2\pi/n},k_z) \\ \exp\left[i\frac{2\pi}{n}(q-r)\right]g_\pm(k_\pm,k_z) &= g_\pm(k_\pm e^{\pm i2\pi/n},k_z) \end{aligned} \tag{A4}$$

where $k_\pm = k_x \pm ik_y$, $g_{0\pm z} = g_0 \pm g_z$.

On k_z axis, these constraints become

$$\begin{aligned} f_z(k_z) &= f_z(k_z) \\ \exp\left[i\frac{2\pi}{n}(p-q)\right]f_+(k_z) &= f_+(k_z) \\ \exp\left[i\frac{2\pi}{n}(p-r)\right]g_{0+z}(k_z) &= g_{0+z}(k_z) \\ \exp\left[i\frac{2\pi}{n}(q-s)\right]g_{0-z}(k_z) &= g_{0-z}(k_z) \\ \exp\left[i\frac{2\pi}{n}(q-r)\right]g_\pm(k_z) &= g_\pm(k_z). \end{aligned} \tag{A5}$$

After considering all other symmetry operations (e.g., reflection symmetry in C), if nondiagonal f,g terms aren't eliminated on the k_z axis, the corresponding (p,q,r,s) pairs (f_+ to p,q, g_0+g_z to p,r, g_0-g_z to q,s, $g_\pm$ to q,r) should be unequal to obtain Dirac points. For example, if f_+ exists on the k_z axis, we should apply $p \neq q$ or a gap will open on the k_z axis.

In order to get the dispersion relation near Dirac points, we should write the f,g terms in a more explicit form. The matrix elements can be expanded as polynomial [59]:

$$f(k_+,k_-) = \sum_{n_1,n_2} A_{n_1n_2}k_+^{n_1}k_-^{n_2}. \tag{A6}$$

Combined with the constraint relations (A4), we obtain

$$\begin{aligned} e^{i2\pi(p-q)/n}f(k_+,k_-) &= f(k_+e^{i2\pi/n},k_-e^{-i2\pi/n}) \\ &= \sum_{n_1,n_2}\exp\left[i\frac{2\pi}{n}(n_1-n_2)\right]A_{n_1n_2}k_+^{n_1}k_-^{n_2} \end{aligned} \tag{A7}$$

where $A_{n_1 n_2}$ is a complex coefficient. To satisfy equations above, the phase factors must cancel each other, i.e., $n_1 - n_2 = (p-q) \bmod n$. We choose the leading order terms to complete Tables I and II. For example, in the C_4 system with $p=3$ and $q=2$, the constraint relation of f_+ term is

$$\exp\left(i\frac{2\pi}{n}\right) f_+(k_\pm,k_z) = f_+(k_\pm e^{\pm i2\pi/n},k_z). \tag{A8}$$

Obviously the leading order term is given by $n_1 = 1, n_2 = 0$, and so we can replace the f_+ term by $A_{1,0}k_+$, neglecting the higher order terms.

APPENDIX B: EXAMPLES OF REFLECTION SYMMETRY OPERATORS

We study the general classification of reflection symmetry operators. The matrix representation of reflection symmetry can be decomposed to orbital and spin space. The reflection operators are not the same as the intuitive ones because of the phase factor stemming from spin. In spin space, reflection operator is a twofold rotation perpendicular to the mirror plane $\hat{n}$: $R_{\pi/2}(\hat{n}) = e^{-i\hat{\sigma} j\cdot\hat{n}\pi/2}$, where j indicates the half-integer spin momentum. At the same time, reflection operators should satisfy the following constraints: (1) $[M,T]=0$, (2) $M^+M=1$, (3) $MM=e^{i\phi}$. Since we only consider four energy bands, the reflection operators can be decomposed to the orbital space τ and spin space σ. Therefore, any four by four matrix $M = (t_0\tau_0 + \vec{t}\cdot\vec{\tau})\otimes(s_0\sigma_0 + \vec{s}\cdot\vec{\sigma})$ satisfying the above (1)–(3) constraints is a reflection operator, where $t_{0,x,y,z}$ and $s_{0,x,y,z}$ are complex numbers. If we set the mirror plane as the yz plane or xy plane, the reflection operators can take four possible forms: (A) $M_k = \pm\tau_0 \otimes i\sigma_k$, (B) $M_k = \pm\tau_z\otimes i\sigma_k$, (C) $M_k = \pm\tau_x\otimes i\sigma_k$, and (D) $M_k = \pm i\tau_y\otimes i\sigma_k (k=x,z)$.

As is shown in Fig. 1, physically there are two classes of mirrors, the mirror parallel and perpendicular to the rotation axis, respectively, corresponds to $k=x$ and $k=z$ above. We can now give the physical examples of these reflection operators. In the following the p orbital states along $x(y)$ direction $|P_{\Lambda x(y)\sigma}\rangle$ compose the angular momentum eigenstates $|P_{\Lambda\pm\sigma}\rangle = |P_{\Lambda x\sigma}\rangle \pm i|P_{\Lambda y\sigma}\rangle$ up to a phase factor, where $\Lambda = A,B$ represents two inequivalent atom sites (see Fig. 1), and $\sigma = \uparrow,\downarrow$ represents spin up and down. For a system with unit cell consisting of two atoms A and B, each atom with two orbitals and two spins, the number of basis is eight. We only consider the four basis composing Dirac point in the low energy effective model and ignored the other four basis that are irrelevant, which is often used when modeling energy bands [60]. The four basis we considered form complete representations of the symmetry operations.

(1) We set the four basis vectors as $(|P_{A+\uparrow}\rangle, |P_{A-\uparrow}\rangle, |P_{A-\downarrow}\rangle, |P_{A+\downarrow}\rangle)$. Then the yz-plane reflection operation interchange P_+,P_- and $\uparrow,\downarrow$, i.e., the reflection operation $M_x : |P_{A+\downarrow}\rangle \to -i|P_{A-\uparrow}\rangle, |P_{A+\uparrow}\rangle \to -i|P_{A-\downarrow}\rangle, |P_{A-\uparrow}\rangle \to -i|P_{A+\downarrow}\rangle, |P_{A-\downarrow}\rangle \to -i|P_{A+\uparrow}\rangle$. The matrix representation of reflection operator is $M_x = -\tau_0\otimes i\sigma_x$.

(2) We set the four basis vectors as $(|P_{A+\downarrow}\rangle, |P_{B+\downarrow}\rangle, -|P_{A-\uparrow}\rangle, -|P_{B-\uparrow}\rangle)$. A glide plane reflection operator can have the following transformation $M_z : |P_{A+\downarrow}\rangle \to -i|P_{B+\downarrow}\rangle$, $|P_{B+\downarrow}\rangle \to -i|P_{A+\downarrow}\rangle$, $|P_{A-\uparrow}\rangle \to i|P_{B-\uparrow}\rangle$, $|P_{B-\uparrow}\rangle \to i|P_{A-\uparrow}\rangle$. Therefore the matrix representation of reflection operator is $M_z = \pm\tau_x\otimes i\sigma_z$.

In general basis for this reflection operator can be constructed as following: There are two inequivalent sites (A and B) and the distance between them is $\vec{t}$. This transformation can be provided by setting: $|P_{A\pm\uparrow(\downarrow)}\rangle = e^{\pm i\vec{r}\cdot\vec{K}} u_{A\pm\uparrow(\downarrow)}, |P_{B\pm\uparrow(\downarrow)}\rangle = e^{\pm iM\vec{r}\cdot\vec{K}} u_{B\pm\uparrow(\downarrow)}$, where $\vec{K}$ denotes the point in Brillouin zone, $u_{A\pm}(M\vec{r}+\vec{t})e^{\pm i\vec{t}\cdot\vec{K}} = u_{B\pm}(\vec{r})$, and $u_A(\vec{r} + M\vec{t} + \vec{t}) = u_A(\vec{r})$. $M_z : \vec{r} \to M\vec{r} + \vec{t}$, where M is a symmorphic reflection operation acting on $\vec{k}$ space and $\vec{K}\cdot(M\vec{t}+\vec{t}) = 2\pi n$. For BiO_2 of space group #227, the Dirac point appears in the X point of its Brillouin zone with reflection symmetry belong to this case.

(3) We set the four basis vectors as $(|P_{A+\uparrow}\rangle, |P_{A+\downarrow}\rangle, |P_{A-\downarrow}\rangle, -|P_{A-\uparrow}\rangle)$ yz-plane reflection operation $M_x : |P_{A+\downarrow}\rangle \to -i|P_{A-\uparrow}\rangle$, $|P_{A+\uparrow}\rangle \to -i|P_{A-\downarrow}\rangle$, $|P_{A-\uparrow}\rangle \to -i|P_{A+\downarrow}\rangle, |P_{A-\downarrow}\rangle \to -i|P_{A+\uparrow}\rangle$ has a matrix form $M_x = -\tau_z\otimes i\sigma_x$.

(4) We set the four basis vectors as $(|P_{A+\downarrow}\rangle, |P_{B+\downarrow}\rangle, -|P_{A-\uparrow}\rangle, -|P_{B-\uparrow}\rangle)$. The reflection operation on the xy plane writes $M_z : |P_{A+\downarrow}\rangle \to i|P_{B+\downarrow}\rangle, |P_{B+\downarrow}\rangle \to -i|P_{A+\downarrow}\rangle, |P_{A-\uparrow}\rangle \to -i|P_{B-\uparrow}\rangle, |P_{B-\uparrow}\rangle \to i|P_{A-\uparrow}\rangle$, with a matrix representation $M_z = i\tau_y\otimes i\sigma_z$. This transformation can be provided when $\vec{K}\cdot(M\vec{t}+\vec{t}) = (2n+1)\pi$ in the same setting of the second example. For $SrIrO_3$ of space group #62, Dirac line node is located around point $U(0,\pi,\pi)$ of the mirror plane $k_y = \pi$ [6,23], with reflection symmetry $(x,y,z) \to (x+\frac{a}{2}, -y+\frac{b}{2}, z+\frac{c}{2})$ satisfying $\vec{K}\cdot(M\vec{t}+\vec{t}) = (2n+1)\pi$, which belongs to this type of reflection.

APPENDIX C: DIRAC POINTS PROTECTED BY REFLECTION AND ROTATIONAL SYMMETRY

The phase transition between normal insulator and WTI/TCI which will generate ABC are shown in Fig. 1(b). When the $p=q$ the bands will feel strong level repulsion and open a gap Fig. 1(c). Here we show the detailed calculation on how Dirac points on k_z axis are protected by reflection and rotational symmetry.

Mirror plane parallel to k_z axis: First we set the mirror plane as the yz plane and the reflection operator as M_x. The combination of M_x and n-fold rotation operation generates $n-1$ more mirror planes and therefore all these reflection operators can be denoted as $M_k = C_n^k M_x (k=0,1,\ldots,n-1)$. These mirror planes cross on k_z axis and confine the Hamiltonian in the k_z axis. For each M_k, there's commutation relation $M_k H(k_z) M_k^{-1} = H(k_z)$. For the situation where $pqrs$ are chosen to eliminate off diagonal f,g terms according to constraint relations (A5), when $M_x = \tau_0/\tau_z\otimes i\sigma_x$, the Hamiltonian becomes $H(k_z) = \mathrm{diag}[a_0+a_{30}, a_0-a_{30}, a_0+a_{30}, a_0-a_{30}]$; when $M_x = \tau_x/i\tau_y\otimes i\sigma_x$, the Hamiltonian becomes $H(k_z) = \mathrm{diag}[a_0+a_{33}, a_0-a_{33}, a_0+a_{33}, a_0-a_{33}]$. It is notable that at time reversal invariant momentum (TRIM) all a terms with odd parity are eliminated due to the relation $[H,T]=0$ and only $a_{00}, a_{10}, a_{30}, a_{21}, a_{22}, a_{23}$ survive. Therefore, the constraints on (p,q,r,s) are less in TBC [see Fig. 1(d)]. All the results of the physical properties of Dirac semimetal are shown in Table I.

Mirror plane perpendicular to k_z axis: First we set the mirror plane as the xy plane and the reflection operator as M_z. Along the k_z axis, the reflection symmetry is $M_z H(k_z) M_z^{-1} = H(-k_z)$. Combined with C_2, C_4, C_6 rotational symmetry, reflection symmetry can create inversion symmetry $P = M_z \hat{C}_2$. The rotation operator for orbital space is $C_n = i\exp(i\pi\frac{1+p+q}{n})\exp(i\pi\frac{p-q}{n}\tau_z) = i\exp(i\pi\frac{1+p+q}{n})[\cos\frac{\pi}{n}(p-q) + i\tau_z\sin\frac{\pi}{n}(p-q)]$. Twofold rotation is $\hat{C}_2 = \cos\theta\tau_0 + \sin\theta\tau_z$ where $\theta = \frac{\pi}{2}(p-q)$. If $p-q = 0,2,4$, then $\hat{C}_2 = \pm\tau_0$. These conditions can be satisfied when $p = q$ for C_2 symmetry, when $p = q$ or $p = q+2$ for C_4 symmetry, when $p = q$, $p = q+2$ or $p = q+4$ for C_6 symmetry. If $p - q = 1,3,5$, then $\hat{C}_2 = \pm\tau_z$. These conditions can be satisfied when $p = 1, q = 0$ for C_2 symmetry, when $p = q+1$ or $p = q+3$ for C_4 symmetry, when $p = q+1$, $p = q+3$ or $p = q+5$ for C_6 symmetry. The symmetry constraints with TRS along the k_z axis are $M_z H(k_z) M_z^{-1} = TH(k_z)T^{-1}$ and $PH(k_z)P^{-1} = TH(k_z)T^{-1}$. After constraint relations (A5) are applied for the nonzero a terms, all situations protecting Dirac points are shown in Table II, holding the same results as Yang and Nagaosa [40] when $P = \pm\tau_0, \pm\tau_z, \pm\tau_x$. When $P = \pm i\tau_y$ the system can also generate Dirac points. For C_3 symmetry, the system does not have inversion symmetry. We only have symmetry constraints $M_z H(k_z) M_z^{-1} = TH(k_z)T^{-1}$ together with constraint relations (A5) and the result is shown in Table III.

APPENDIX D: $k \cdot p$ MODEL OF C_{4v} GROUP

In this section, we use the four band model to describe the effective Hamiltonian of material with point group C_{4v} such as Cd_3As_2. We write the 4×4 effective Hamiltonian generally as:

$$H_{\text{eff}} = \sum_{i,j=0}^{3} d_{ij}(k)\Gamma_{ij} \tag{D1}$$

where $\Gamma_{ij} = \tau_i\sigma_j$. The basis vectors of effective Hamiltonian are four angular momentum eigenstates $|+\frac{1}{2}\rangle, |+\frac{3}{2}\rangle, |-\frac{1}{2}\rangle$, and $|-\frac{3}{2}\rangle$, among which $(|+\frac{1}{2}\rangle, |-\frac{1}{2}\rangle)$ belongs to $\tilde{\Gamma}_6$ representation and $(|+\frac{3}{2}\rangle, |-\frac{3}{2}\rangle)$ belongs to $\tilde{\Gamma}_7$ representation.

Then we investigate the representations of Γ matrices and k polynomials with three symmetric operations: the fourfold rotation along Z axis $\hat{C}_4$, the vertical reflection $\hat{m}_v$, and the dihedral reflection $\hat{m}_d = \hat{C}_4\hat{m}_v$. The matrix operation of these symmetric operators are: (1) $U(\hat{C}_4) = R_{\frac{1}{2}}(\hat{C}_4) \oplus R_{\frac{3}{2}}(\hat{C}_4)$, (2) $U(\hat{m}_v) = R_{\frac{1}{2}}(\hat{m}_v) \oplus R_{\frac{3}{2}}(\hat{m}_v)$, and (3) $U(\hat{m}_d) = U(\hat{m}_v)U(\hat{C}_4)$, where $R_j(\hat{C}_4) = \exp(i\frac{\pi}{2}j\sigma_z)$, $R_j(\hat{m}_v) = \exp(i\frac{\pi}{2}j\sigma_x)$.

The operators act on the k polynomials $d_{ij}(k)$ as: (1) $\hat{C}_4 : k_x \to -k_y, k_y \to k_x, k_z \to k_z$, (2) $\hat{m}_v : k_x \to -k_x, k_y \to k_y, k_z \to k_z$, (3) $\hat{m}_d : k_x \to k_y, k_y \to k_x, k_z \to k_z$.

The representations of Γ matrices and k polynomials $d(k)$ are shown in Table V. Knowing the multiplication relations of representations $\tilde{\Gamma}_6 \otimes \tilde{\Gamma}_6 = \tilde{\Gamma}_1 \oplus \tilde{\Gamma}_2 \oplus \tilde{\Gamma}_5, \tilde{\Gamma}_7 \otimes \tilde{\Gamma}_7 = \tilde{\Gamma}_1 \oplus \tilde{\Gamma}_2 \oplus \tilde{\Gamma}_5, \tilde{\Gamma}_6 \otimes \tilde{\Gamma}_7 = \tilde{\Gamma}_3 \oplus \tilde{\Gamma}_4 \oplus \tilde{\Gamma}_5$, by assembling the Γ matrices and $d(k)$ with the same representation and TRS eigenvalue we obtain our effective Hamiltonian:

TABLE V. The representations of C_{4v} group with Γ matrices and k polynomials

Reps	Γ matrices	$d(k)$	T
$\tilde{\Gamma}_1$	Γ_{00}, Γ_{30}	$1, k_x^2 + k_y^2, k_z^2$	+
$\tilde{\Gamma}_1$		k_z	−
$\tilde{\Gamma}_2$	Γ_{03}, Γ_{33}		−
$\tilde{\Gamma}_3$	Γ_{22}	$k_x^2 - k_y^2$	+
$\tilde{\Gamma}_3$	Γ_{12}		−
$\tilde{\Gamma}_4$	Γ_{21}	$k_x k_y$	+
$\tilde{\Gamma}_4$	Γ_{11}		−
$\tilde{\Gamma}_5$	$(\Gamma_{10}, \Gamma_{23})$	$(k_x k_z, k_y k_z)$	+
$\tilde{\Gamma}_5$	$(\Gamma_{32}, \Gamma_{01}), (\Gamma_{02}, \Gamma_{31}), (\Gamma_{20}, -\Gamma_{13})$	(k_x, k_y)	−

$$H_{\text{eff}}(\vec{k}) = \epsilon(\vec{k}) + \begin{pmatrix} A(\vec{k}) & -D(\vec{k})k_+ & B_+k_- & -C(\vec{k}) \\ -D^*(\vec{k})k_- & -A(\vec{k}) & C(\vec{k}) & B_-k_+ \\ B_+k_+ & C^*(\vec{k}) & A(\vec{k}) & D(\vec{k})k_- \\ -C^*(\vec{k}) & B_-k_- & D^*(\vec{k})k_+ & -A(\vec{k}) \end{pmatrix}. \tag{D2}$$

In Eqs. (D2) $\epsilon(\vec{k}) = E_0 + E_1k_+k_- + E_2k_z^2$, $A(\vec{k}) = A_0 + A_1k_+k_- + \sqrt{A_2k_z^2 + A_{20}^2}$, $B_\pm = \pm B_0 + B_1$, $C(\vec{k}) = \frac{C_0}{2}(k_+^2 + k_-^2) + \frac{i}{4}C_1(k_+^2 - k_-^2)$, $D(\vec{k}) = D_0 + iD_1k_z$, and $k_\pm = k_x \pm ik_y$.

The Hamiltonian (D2) shows the possibility of coexistence of 3D Dirac points and Weyl line nodes (WLNs). By choosing proper parameters shown in Table VI (only B_0 is different from Cd_3As_2) we can verify our statement through the band structure Fig. 3(a). This figure is accomplished with the substitutions: $k_i \to \frac{1}{L_i}\sin(k_iL_i), k_i^2 \to \frac{2}{L_i^2}[1 - \cos(k_iL_i)]$ for a periodic lattice, where $L_x = L_y = a = 12.67$ Å and $L_z = c = 25.48$ Å [18].

In order to solve WLNs, it is convenient to neglect the symmetric terms $\epsilon(\vec{k})$ and some parameters B_1, C_0, C_1, D_1 as is shown in Table VI. Therefore, explicit calculation gives the equation of WLNs:

$$\left(B_0^2 - D_0^2\right)k_x^2 = \left[A_0 + A_1k_x^2 + \sqrt{A_2k_z^2 + A_{20}^2}\right]^2. \tag{D3}$$

This is schematically shown in Fig. 3(b).

TABLE VI. Parameters for the 4×4 effective Hamiltonian [Eq. (D2)]. Most parameters can be referred to from Jeon, Sangjun *et al.* [19].

E_0 (eV)	−0.219	B_0(eVÅ)	5
E_1 (eVÅ^2)	−30	B_1(eVÅ)	0
E_2 (eVÅ^2)	−16	C_0(eVÅ^2)	0
A_0 (eV)	−0.060	C_1(eVÅ^2)	0
A_1 (eVÅ^2)	18	D_0(eVÅ)	−2.75
A_2 (eV^{2}Å^2)	96	D_1(eVÅ^2)	0
A_{20} (eV^2)	0.050		

In Fig. 3, the B_1, C_0, C_1, D_1 terms are neglected. B_0 and D_0 are two main parameters determining whether there is a gap or WLNs in Brillouin zone. The phase diagram of B_0 and D_0 is shown in Fig. 3(c). The critical line where WLNs appear and disappear is close to the line $D_0 = B_0$, but B_0 is actually slightly larger than D_0, which can be shown more clearly with a smaller A_0 [see Fig. 3(c) the dark blue area]. On the critical line, the two bands pull apart and the WLNs eventually annihilate accompanied by opening a gap.

[1] X.-L. Qi and S.-C. Zhang, Rev. Mod. Phys. **83**, 1057 (2011).
[2] M. Z. Hasan and C. L. Kane, Rev. Mod. Phys. **82**, 3045 (2010).
[3] S. M. Young, S. Zaheer, J. C. Y. Teo, C. L. Kane, E. J. Mele, and A. M. Rappe, Phys. Rev. Lett. **108**, 140405 (2012).
[4] S. M. Young and C. L. Kane, Phys. Rev. Lett. **115**, 126803 (2015).
[5] Z. Wang, Y. Sun, X.-Q. Chen, C. Franchini, G. Xu, H. Weng, X. Dai, and Z. Fang, Phys. Rev. B **85**, 195320 (2012).
[6] J.-M. Carter, V. V. Shankar, M. A. Zeb, and H.-Y. Kee, Phys. Rev. B **85**, 115105 (2012).
[7] H.-S. Kim, Y. Chen, and H.-Y. Kee, Phys. Rev. B **91**, 235103 (2015).
[8] Y. Chen, Y.-M. Lu, and H.-Y. Kee, Nat. Commun. **6**, 6593 (2015).
[9] J.-W. Rhim and Y. B. Kim, Phys. Rev. B **92**, 045126 (2015).
[10] H. Weng, Y. Liang, Q. Xu, R. Yu, Z. Fang, X. Dai, and Y. Kawazoe, Phys. Rev. B **92**, 045108 (2015).
[11] M. Zeng, C. Fang, G. Chang, Y.-A. Chen, T. Hsieh, A. Bansil, H. Lin, and L. Fu, arXiv:1504.03492.
[12] R. Yu, H. Weng, Z. Fang, X. Dai, and X. Hu, Phys. Rev. Lett. **115**, 036807 (2015).
[13] Y. Kim, B. J. Wieder, C. L. Kane, and A. M. Rappe, Phys. Rev. Lett. **115**, 036806 (2015).
[14] M. Franz and L. Molenkamp, *Topological Insulators*, Vol. 6 (Elsevier, Amsterdam, 2013).
[15] T. Morimoto and A. Furusaki, Phys. Rev. B **89**, 235127 (2014).
[16] B. Büttner, C. Liu, G. Tkachov, E. Novik, C. Brüne, H. Buhmann, E. Hankiewicz, P. Recher, B. Trauzettel, S. Zhang *et al.*, Nat. Phys. **7**, 418 (2011).
[17] Z. Wang, H. Weng, Q. Wu, X. Dai, and Z. Fang, Phys. Rev. B **88**, 125427 (2013).
[18] M. Neupane, S.-Y. Xu, R. Sankar, N. Alidoust, G. Bian, C. Liu, I. Belopolski, T.-R. Chang, H.-T. Jeng, H. Lin *et al.*, Nat. Commun. **5**, 3786 (2014).
[19] S. Jeon, B. B. Zhou, A. Gyenis, B. E. Feldman, I. Kimchi, A. C. Potter, Q. D. Gibson, R. J. Cava, A. Vishwanath, and A. Yazdani, Nat. Mater. **13**, 851 (2014).
[20] Z. Liu, J. Jiang, B. Zhou, Z. Wang, Y. Zhang, H. Weng, D. Prabhakaran, S. Mo, H. Peng, P. Dudin *et al.*, Nat. Mater. **13**, 677 (2014).
[21] M. N. Ali, Q. Gibson, S. Jeon, B. B. Zhou, A. Yazdani, and R. Cava, Inorg. Chem. **53**, 4062 (2014).
[22] Z. K. Liu, B. Zhou, Y. Zhang, Z. J. Wang, H. M. Weng, D. Prabhakaran, S.-K. Mo, Z. X. Shen, Z. Fang, X. Dai, Z. Hussain, and Y. L. Chen, Science **343**, 864 (2014).
[23] C. Fang, Y. Chen, H.-Y. Kee, and L. Fu, Phys. Rev. B **92**, 081201 (2015).
[24] G. Xu, H. Weng, Z. Wang, X. Dai, and Z. Fang, Phys. Rev. Lett. **107**, 186806 (2011).
[25] X. Wan, A. M. Turner, A. Vishwanath, and S. Y. Savrasov, Phys. Rev. B **83**, 205101 (2011).
[26] H. Zhang, J. Wang, G. Xu, Y. Xu, and S.-C. Zhang, Phys. Rev. Lett. **112**, 096804 (2014).
[27] H. Weng, C. Fang, Z. Fang, B. A. Bernevig, and X. Dai, Phys. Rev. X **5**, 011029 (2015).
[28] S.-M. Huang, S.-Y. Xu, I. Belopolski, C.-C. Lee, G. Chang, B. Wang, N. Alidoust, G. Bian, M. Neupane, C. Zhang *et al.*, Nat. Commun. **6**, 7373 (2015).
[29] S.-Y. Xu, I. Belopolski, N. Alidoust, M. Neupane, G. Bian, C. Zhang, R. Sankar, G. Chang, Z. Yuan, C.-C. Lee, S.-M. Huang, H. Zheng, J. Ma, D. S. Sanchez, B. Wang, A. Bansil, F. Chou, P. P. Shibayev, H. Lin, S. Jia, and M. Z. Hasan, Science **349**, 613 (2015).
[30] B. Q. Lv, H. M. Weng, B. B. Fu, X. P. Wang, H. Miao, J. Ma, P. Richard, X. C. Huang, L. X. Zhao, G. F. Chen, Z. Fang, X. Dai, T. Qian, and H. Ding, Phys. Rev. X **5**, 031013 (2015).
[31] B. Q. Lv, N. Xu, H. Weng, J. Ma, P. Richard, X. Huang, L. Zhao, G. Chen, C. Matt, F. Bisti *et al.*, Nat. Phys. **11**, 724 (2015).
[32] X. Yang, Y. Li, Z. Wang, Y. Zhen, and Z.-a. Xu, arXiv:1506.02283.
[33] L. Yang, Z. Liu, Y. Sun, H. Peng, H. Yang, T. Zhang, B. Zhou, Y. Zhang, Y. Guo, M. Rahn *et al.*, Nat. Phys. **11**, 728 (2015).
[34] S.-Y. Xu, N. Alidoust, I. Belopolski, Z. Yuan, G. Bian, T.-R. Chang, H. Zheng, V. N. Strocov, D. S. Sanchez, G. Chang *et al.*, Nat. Phys. **11**, 748 (2015).
[35] C. Shekhar, A. K. Nayak, Y. Sun, M. Schmidt, M. Nicklas, I. Leermakers, U. Zeitler, Y. Skourski, J. Wosnitza, Z. Liu *et al.*, Nat. Phys. **11**, 645 (2015).
[36] C. Shekhar, F. Arnold, S.-C. Wu, Y. Sun, M. Schmidt, N. Kumar, A. G. Grushin, J. H. Bardarson, R. D. d. Reis, M. Naumann *et al.*, arXiv:1506.06577.
[37] C. Zhang, Z. Yuan, S. Xu, Z. Lin, B. Tong, M. Z. Hasan, J. Wang, C. Zhang, and S. Jia, arXiv:1502.00251.
[38] X. Huang, L. Zhao, Y. Long, P. Wang, D. Chen, Z. Yang, H. Liang, M. Xue, H. Weng, Z. Fang, X. Dai, and G. Chen, Phys. Rev. X **5**, 031023 (2015).
[39] A. A. Soluyanov, D. Gresch, Z. Wang, Q. Wu, M. Troyer, X. Dai, and B. A. Bernevig, Nature (London) **527**, 495 (2015).
[40] B.-J. Yang and N. Nagaosa, Nat. Commun. **5**, 4898 (2014).
[41] C.-K. Chiu, H. Yao, and S. Ryu, Phys. Rev. B **88**, 075142 (2013).
[42] C.-K. Chiu and A. P. Schnyder, Phys. Rev. B **90**, 205136 (2014).
[43] C.-K. Chiu, J. C. Teo, A. P. Schnyder, and S. Ryu, arXiv:1505.03535.
[44] B. A. Bernevig and T. L. Hughes, *Topological insulators and topological superconductors* (Princeton University Press, Princeton and Oxford, 2013).
[45] J. A. Steinberg, S. M. Young, S. Zaheer, C. L. Kane, E. J. Mele, and A. M. Rappe, Phys. Rev. Lett. **112**, 036403 (2014).
[46] R. S. K. Mong, J. H. Bardarson, and J. E. Moore, Phys. Rev. Lett. **108**, 076804 (2012).
[47] C.-X. Liu, X.-L. Qi, and S.-C. Zhang, Physica E **44**, 906 (2012).

[48] Z. Ringel, Y. E. Kraus, and A. Stern, Phys. Rev. B **86**, 045102 (2012).

[49] L. Fu, Phys. Rev. Lett. **106**, 106802 (2011).

[50] T. H. Hsieh, H. Lin, J. Liu, W. Duan, A. Bansil, and L. Fu, Nat. Commun. **3**, 982 (2012).

[51] B. A. Bernevig, T. L. Hughes, and S.-C. Zhang, Science **314**, 1757 (2006).

[52] A. A. Burkov and L. Balents, Phys. Rev. Lett. **107**, 127205 (2011).

[53] P. Hosur, S. A. Parameswaran, and A. Vishwanath, Phys. Rev. Lett. **108**, 046602 (2012).

[54] C.-X. Liu, P. Ye, and X.-L. Qi, Phys. Rev. B **87**, 235306 (2013).

[55] M. M. Vazifeh and M. Franz, Phys. Rev. Lett. **111**, 027201 (2013).

[56] A. C. Potter, I. Kimchi, and A. Vishwanath, Nat. Commun. **5**, 5161 (2014).

[57] S. A. Yang, H. Pan, and F. Zhang, Phys. Rev. Lett. **113**, 046401 (2014).

[58] C. H. Lee, X. Zhang, and B. Guan, Sci. Rep. **5**, 18008 (2015).

[59] C. Fang, M. J. Gilbert, X. Dai, and B. A. Bernevig, Phys. Rev. Lett. **108**, 266802 (2012).

[60] P. Y. Yu and M. Cardona, *Fundamentals of Semiconductors* (Springer, Berlin, 2005).